FUSION-ALPHA-ENHANCED DISPLACEMENT AND STABILITY OF ITER HELICAL CORE PLASMAS

P. ADULSIRISWAD, A. BIERWAGE, M. YAGI

National Institute for Quantum Science and Technology (QST), Rokkasho Institute for Fusion Energy Rokkasho, Aomori, Japan

Email: adulsiriswad.panith@qst.go.jp

Abstract

The transition from an axisymmetric equilibrium to a helical core (HC)—a three-dimensional magnetohydrodynamic (MHD) equilibrium characterized by a tilted magnetic axis with both toroidal and poloidal periodicities of unity—is studied in the ITER-scale hybrid scenario. This study examines the effects of fusion-born alphas using a global MHD-particle-in-cell (PIC) simulation code. The HC state is determined by a toroidally asymmetric MHD force balance, which depends on the given plasma's parameters, such as the safety factor profile and the total pressure profile of all particle species. In examining the role of alphas, we observe that the core toroidal asymmetry, represented here by the n=1 displacement of the magnetic axis δ_{HC} , increases with alpha pressure β_{α} within the reference ITER operating range, $\beta_{\alpha} \leq 1\%$. Here, the contribution of alphas to the steady state δ_{HC} can be well approximated using a fluid model because the HC state is determined mainly by the minimization of the ideal MHD energy. The fluid model may only miss mode rotation from alpha diamagnetic and resonant effects. If β_{α} is raised above the nominal ITER operating range, $\beta_{\alpha} > 1\%$, δ_{HC} will continue to increase until it reaches an upper limit, where the MHD HC transform into an energetic particle-driven mode, and eventually transport confinement and stability begin to fall. The ideal fluid approximation of alphas becomes invalid, necessitating the use of a kinetic model. Irrespective of the presence of alphas, we observed the destabilization of the short-wavelength MHD mode, localized along the compressed flux region of HC. Our preliminary results, which remain to be confirmed with micro-turbulence codes, suggest that the secondary mode may lead to a significant chaotization of the magnetic field, affecting both the bulk plasma and alpha confinements.

1. INTRODUCTION

A tokamak hybrid scenario is characterized by weak core magnetic shear, with a safety factor slightly above unity, $q \gtrsim 1$. This scenario features strong plasma self-organization driven by the benign m/n=1/1 non-resonant kink/quasi-interchange mode, which helps to sustain a sawtooth-free plasma with minimal to no external control. However, this mode can ideally be saturated, leading to a long-lived toroidally asymmetric equilibrium state known as a helical core (HC)[1, 2]. The illustration of the HC state in ITER-scale plasmas is shown in Fig.1. Panel (a) shows a 3-D view of the HC magnetic flux surfaces where the red solid line, black dotted line, the red surface, and the gray surface represent the HC magnetic axis, the planar axis, an arbitrary flux surface within the $q \gtrsim 1$ region, and the last closed flux surface, respectively. The magnetic axis (red solid line) is tilted with respect to the planar axis, and the flux surface inside the $q \gtrsim 1$ region (red surface) is helically distorted with the toroidal and poloidal periodicities of unity (m/n=1/1). The magnetic Poincaré plots at the $\phi=0^\circ$ and 180° toroidal angles are shown in panels (b) and (c), respectively. The displacement of flux surfaces creates a poloidal region where the flux surfaces are moving closer to each other, and consequently, a region where the flux surfaces are moving apart. These poloidal regions refer to the "compressed" and "uncompressed" flux regions, respectively. For clarity, the phase of the HC shown in this study is adjusted so that the compressed flux region is located on the low-field side at $\phi=0^\circ$.

Although HC helps maintain a sawtooth-free plasma, its toroidal asymmetry can affect energetic particle (EP) confinement[3, 4], damping plasma rotation[4], and interfere with plasma diagnostics. In the latter case, HC can shift the core plasma away from diagnostic sight lines initially designed for axisymmetric plasmas, causing the measured plasma conditions to be dependent on the phase of HC. These factors must be considered in the initial design of a hybrid-scenario tokamak reactor, necessitating a comprehensive understanding and accurate prediction of HC formation and structure. Previous studies [1, 5, 6] have utilized VMEC[7], a 3-D equilibrium solver based on ideal MHD energy minimization, to study how the onset and structure of HC depend on (i) plasma shape, (ii) safety factor q profile, and (iii) pressure profile. These studies also predicted the spontaneous formation of HC in ITER with the n=1 magnetic axis displacement of half a meter. Since ITER aims to demonstrate the control of burning plasma, it is predicted that the core plasma will be populated with fusion-born alphas with a normalized pressure of approximately $\beta_{\alpha}=1\%$. Kinetic effects of energetic particles (EPs), such as fusion-born alpha particles, are known to influence the linear stability of the kink/quasi-interchange mode[8, 9], a precursor mode to HC. These alpha particles can modify HC, which in turn globally modifies the magnetic field and affects their confinement. In actual plasmas,

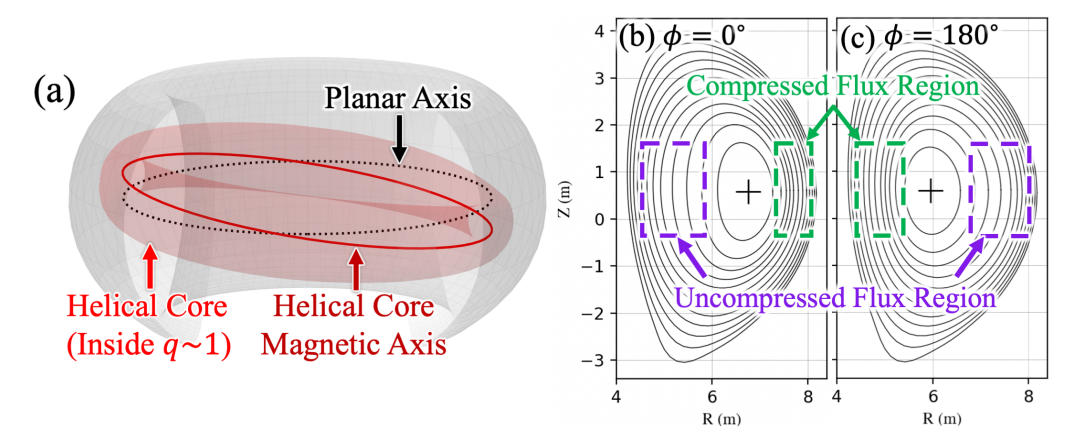


FIG. 1. Illustrations of HC tokamak equilibrium state: (a) 3-D structure of HC. The red solid line and the red surface represent the HC magnetic axis and an arbitrary magnetic flux surface that resides within the $q\sim 1$ region. The gray surface represents the last closed flux surface. (b-c) Magnetic Poincaré plot at $\phi=0^\circ$ and 180° . The compressed and uncompressed flux regions of HC are labeled using violet and green colors, respectively.

HC formation, alpha particle behavior, and heating are simultaneous and mutually coupled. To clarify the role of alphas in this complex interplay, this study begins with a simplified situation, specifically the role of alphas during the onset of the HC state with a prescribed axisymmetric plasma and alpha profiles. This paper is organized as follows. Section 2 introduces the simulation model and plasma parameters. In the first half of Section 3, we verified that our MHD-PIC code, MEGA[10], yields the same results as VMEC in the absence of alphas. The effects of alpha particles are discussed in the second half of that section. Section 4 presents the preliminary results on the MHD stability of HC. Section 5 is then devoted to the conclusion.

2. SIMULATION MODELS AND PLASMA PARAMETERS

2.1. MEGA, a Nonlinear MHD-PIC Code

To simulate the transition from the axisymmetric equilibrium to the HC equilibrium with the kinetic fusion-born alphas, MEGA[10], a global nonlinear PIC-MHD code, is used. The bulk plasma is modeled using resistive MHD equations, while the alphas are modeled using a drift kinetic equation. These two models are coupled via the current-coupling scheme. The set of MHD equations solved by MEGA is shown below.

$$\frac{\partial \rho_M}{\partial t} = -\nabla \cdot (\rho_M \vec{v}) + \nu_n \nabla^2(\rho_M), \tag{1}$$

$$\rho_M \frac{\partial \vec{v}}{\partial t} = -\rho_M(\vec{v} \cdot \nabla)\vec{v} - \nabla P + (\vec{J} - \vec{J}_\alpha) \times \vec{B} - \nabla \times (\nu \rho_M(\nabla \times \vec{v})) + \frac{4}{3}\nabla(\nu \rho_M \nabla \cdot \vec{v}), \tag{2}$$

$$\frac{\partial P}{\partial t} = -\nabla \cdot (P\vec{v}) - (\Gamma - 1)P\nabla \cdot \vec{v} + (\Gamma - 1) \times [\nu \rho_M (\nabla \times \vec{v})^2 + \frac{4}{3}\nu \rho_M (\nabla \cdot \vec{v})^2 + \eta \vec{J} \cdot (\vec{J} - \vec{J}_{eq})] + \chi_{\parallel} \nabla_{\parallel}^2 P + \chi_{\perp} \nabla_{\perp}^2 P, \tag{3}$$

$$\frac{\partial \vec{B}}{\partial t} = -\nabla \times \vec{E} \quad (4), \qquad \mu_0 \vec{J} = \nabla \times \vec{B} \quad (5), \qquad \vec{E} = -\vec{v} \times \vec{B} + \eta (\vec{J} - \vec{J}_{eq}) \quad (6).$$

The definition of each variables are as follows: bulk plasma mass density ρ_M , bulk plasma pressure P, total current density J, total current density at initial equilibrium state J_{eq} , alpha current density J_{α} , MHD velocity \vec{v} , magnetic field \vec{B} , electric field \vec{E} , specific heat ratio Γ , particle diffusivity ν_n , viscosity ν , plasma resistivity η , parallel heat conductivity χ_{\parallel} , and perpendicular heat conductivity χ_{\perp} . The dissipation terms help to maintain numerical stability by dissipating small-scale structures into heat. η is also used to study the resistive effects on HC and its stability. Unless stated otherwise, these dissipation terms are assumed to be spatially uniform with $\nu_n = 10^{-6} v_A R_0$, $\nu = 10^{-6} v_A R_0$, $\eta = 10^{-6} \mu_0 v_A R_0$, $\chi_{\parallel} = 10^{-4} v_A R_0$, and $\chi_{\perp} = 10^{-6} v_A R_0$, where v_A and R_0 are Alfvén velocity and major radius, respectively. It should be noted that $\chi_{\parallel} = 10^{-4} v_A R_0$ is insufficient to capture the rapid parallel transport along the magnetic field line. Using a higher value is computationally inefficient in MEGA because the explicit time integration scheme is used. This limitation slows down the pressure relaxation along the magnetic field line, which prevents the plasma from reaching an ideal MHD equilibrium state within a short simulation time. Therefore,

this code can only simulate the transitional dynamics and, at best, the quasi-steady state of the HC. In addition to this issue, such a low χ_{\parallel} may exaggerate ballooning modes at short wavelengths. MEGA resolves this issue by using a geometrical toroidal low-pass filter that acts along the geometrical toroidal angle ϕ , limiting plasma fluctuations to the specified maximum toroidal mode number $n_{\rm max}$. However, after HC formation, this filter becomes less effective because the geometric toroidal direction at a given (R,Z) intersects multiple flux surfaces.

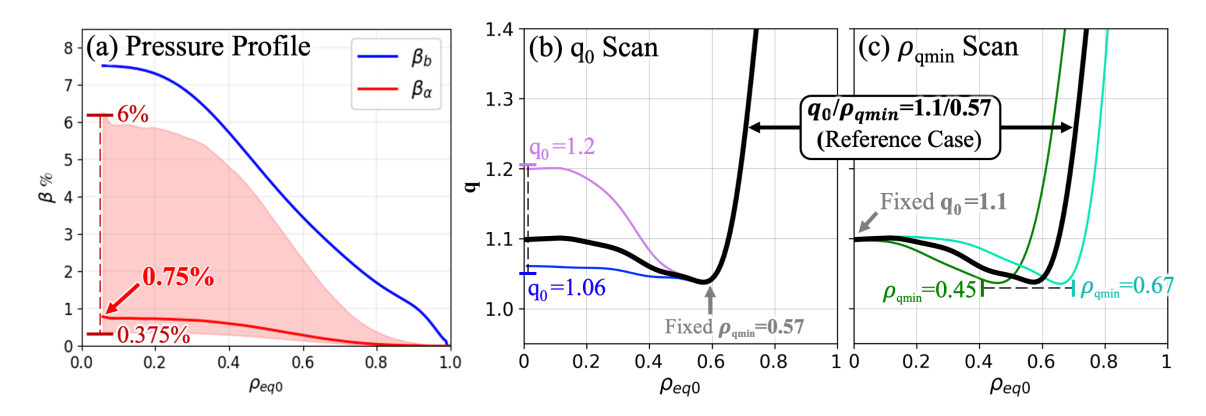


FIG. 2. Initial equilibrium plasma profile conditions for ITER plasmas: (a) Bulk plasma β_b and scanned fusion-born alpha β_{α} pressure profiles; (b-c) Safety factor q profile for the q_0 and ρ_{qmin} scans.

2.2. VMEC, a 3-D Ideal MHD Equilibrium Solver

In addition to MEGA, we also use VMEC[7], a 3-D ideal MHD equilibrium code that has been used to study HC formation in other studies[1, 5, 6]. Unlike MEGA, this code predicts the HC equilibrium state by minimizing the ideal MHD energy functional for specified plasma boundary, pressure profile, and q profile. Since VMEC cannot capture the kinetic effect of alphas, the contribution of alphas is considered only as an additional scalar MHD pressure using

$$\beta_{\text{tot}}(\rho_{\text{eq0}}) = \beta_b(\rho_{eq0}) + \frac{1}{2\pi} \int_0^{2\pi} \beta_\alpha(\rho_{eq0}, \theta) d\theta, \tag{7}$$

where $\beta_{\rm tot}$, β_b , and β_α are total plasma, bulk plasma, and alpha pressures, respectively. $\rho_{\rm eq}$ represents the normalized toroidal flux, while the "0" subscript represents the axisymmetric equilibrium state. The HC solution obtained with this method is equivalent to the solution at the ideal MHD limit with zero flow. Comparing this solution with the MEGA solution can then untangle the kinetic effects of alphas from ideal MHD contributions.

2.3. ITER-Scale MHD Equilibrium and alpha Distribution Function

The axisymmetric reference equilibrium (pressure, density, shape) is based on the ITER hybrid scenario calculated by COR-SICA[11] with the on-axis magnetic field strength and the net plasma current of approximately 5 T and 13 MA, respectively. The $\beta_{\rm b}$ profile is shown in Fig.2(a) with an on-axis value of 7.56%. Here, we treat the safety factor q profile as a free parameter. The main reference equilibrium has a weakly reversed magnetic shear profile with the on-axis safety factor (q_0) of 1.1 and the radial position of $q_{\rm min} = 1.04$ ($\rho_{\rm qmin}$) of 0.57, as shown by the black solid line in Figs.2(b-c). In addition, we consider the scanning of q_0 and $\rho_{\rm qmin}$ exclusively in Section 3.1, where we benchmark the HC solution of MEGA and VMEC in the absence of alpha. These q scans are intended to ensure the agreement between MEGA and VMEC across a broad range of equilibria. The q_0 and $\rho_{\rm qmin}$ profiles used in our scans are shown in Figs.2(b-c), respectively.

For the fusion-born alphas, we assume they have been confined sufficiently long until an isotropic slowing-down energy distribution is established. The total alpha population is then estimated from the D-T fusion reaction within the slowing-down timescale. This yields the β_{α} profile with the on-axis value of 0.75% as shown by the red solid line in Fig.2(a). Additionally, we intend to investigate the sensitivity of HC formation to β_{α} . This β_{α} profile is numerically scaled within the range $0.375\% \le \beta_{\alpha} \le 6\%$, represented as a red ribbon in the same panel.

3. SIMULATION RESULTS OF HELICAL CORE FORMATION

In the first half of this section, we intend to ensure that MEGA can predict a reliable HC state by benchmarking against VMEC. Since VMEC cannot consider the kinetic effect of alpha, they are excluded in the first part. The kinetic effects of alphas will be included in the second half.

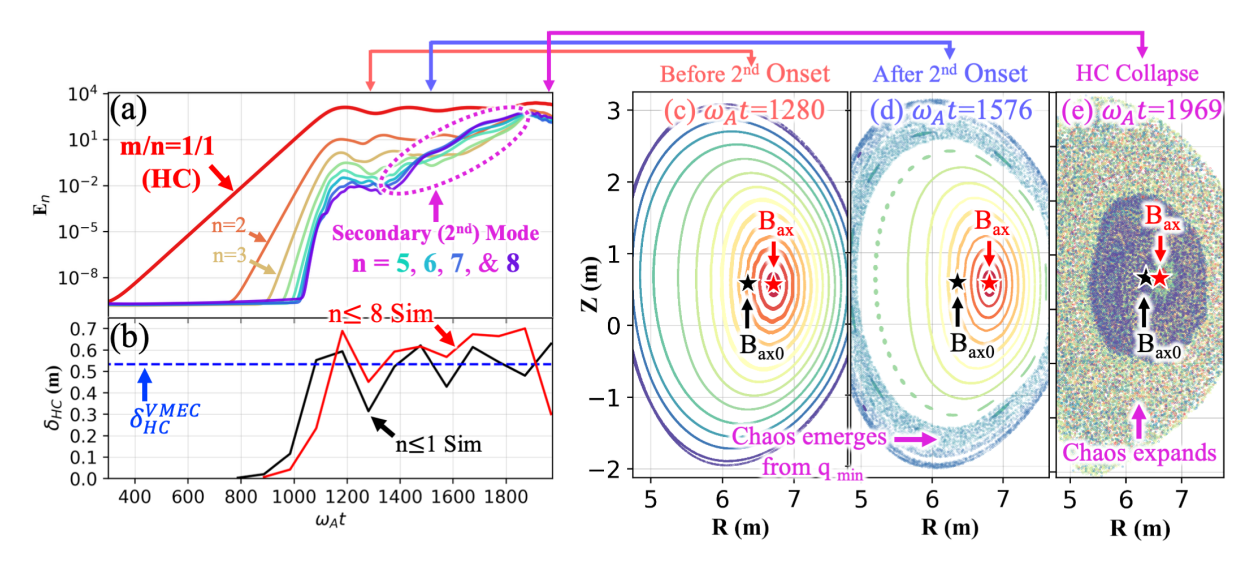


FIG. 3. HC formation for the $q_0/\rho_{\rm qmin}=1.1/0.57$ equilibrium without alphas calculated by MEGA: (a) Time evolution of $1 \le n \le 8$ mode energies; (b) Time evolution of the n=1 magnetic axis displacement $\delta_{\rm HC}$. The black and red solid lines correspond to the MEGA simulation with the $n \le 1$ and $n \le 8$ constraints, respectively, while the horizontal blue dashed line represents the VMEC results; Magnetic Poincaré plots of the HC state calculated with $n \le 8$ constraints at $\phi = 0^{\circ}$ (c) before the onset of secondary mode, (d) shortly after its onset, and (e) near its saturation.

3.1. Benchmarking HC Equilibria with MEGA and VMEC

Firstly, we performed the MEGA simulation constrained to the $n \le 8$ dynamics on the main reference equilibrium $(q_0/\rho_{\rm qmin}=1.1/0.57)$. The time evolution of the mode energies is shown in Figs.3(a), showing that the n=1 mode (red solid line) is the only linearly unstable mode. We confirmed that this n=1 has a single dominant m=1 poloidal harmonic with a quasi-interchange-like eigenfunction. After saturation, the n=1 mode energy is maintained at a non-zero steady-state value, signifying the formation of HC. Besides HC, we observed growth of modes with $1 \le n \le 8$, which we will refer to as "secondary mode" for simplicity.

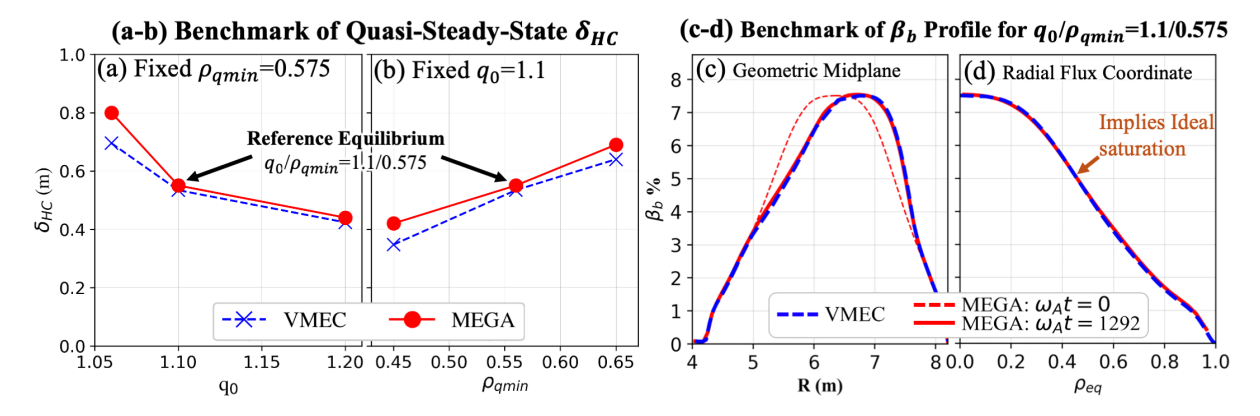


FIG. 4. Comparison of (a-b) δ_{HC} and (c-d) the displaced β_b profiles calculated with MEGA and VMEC. For the comparison of δ_{HC} , panels (a-b) compare the steady-state results for the q_0 and ρ_{qmin} scans, respectively. For comparison of the displaced β_b profiles, panels (c-d) show the β_b profile for the $q_0/\rho_{qmin}=1.1/0.57$ equilibrium, plotted along the geometric mid-plane at $\phi=0^\circ$ in real space and in the radial flux coordinate, respectively.

To benchmark the HC equilibrium computed by MEGA against that of VMEC, we quantify the HC toroidal asymmetry using the n=1 displacement of the magnetic axis, $\delta_{\rm HC}$ defined as

$$\delta_{\rm HC} = \frac{1}{2\pi} \int_0^{2\pi} \sqrt{(R_{ax} - R_{ax0})^2 + (Z_{ax} - Z_{ax0})^2} d\phi. \tag{8}$$

 $R_{\rm ax}$ and $Z_{\rm ax}$ denote the major radial and vertical positions of the magnetic axis. For clarity, $\delta_{\rm HC}$ calculated with MEGA and VMEC are denoted as $\delta_{\rm HC}^{\rm MEGA}$ and $\delta_{\rm HC}^{\rm VMEC}$, respectively. The time evolution of $\delta_{\rm HC}^{\rm MEGA}$ calculated with the $n \leq 8$ simulation is

shown in Fig.3(b) as a red solid line, while $\delta_{\rm HC}^{\rm VMEC}$ is represented by a horizontal blue dashed line. $\delta_{\rm HC}^{\rm MEGA}$ increases from zero and then saturates slightly above $\delta_{\rm HC}^{\rm VMEC}$ for a few hundred Alfvénic times. As time progresses, $\delta_{\rm HC}^{\rm MEGA}$ increases on average until it is abruptly reduced at the end of the simulation, $\omega_A t \sim 1850$. It can be seen that its dynamics correlate with the appearance of the secondary mode shown in Panel (a). To understand the abrupt reduction of $\delta_{\rm HC}^{\rm MEGA}$, we check the magnetic Poincaré plots of the HC state before the onset of secondary mode, shortly after its onset, and near its saturation, as shown in Figs.3(c-e), respectively. Before the onset of the secondary mode, the nested magnetic flux surfaces are preserved. Slightly after the onset of the secondary mode, the magnetic field becomes chaotic near $q_{\rm min}$. As the secondary mode grows further, the magnetic chaos becomes larger until it entirely encompasses the core plasma, leading to the reduction of $\delta_{\rm HC}^{\rm MEGA}$.

To eliminate the contribution of the secondary mode, the $n \leq 1$ MEGA simulation result is shown in Fig.3(b) as a black solid line. Without the secondary mode, the abrupt reduction and nonlinear growth of $\delta_{\rm HC}^{\rm MEGA}$ is not observed, and $\delta_{\rm HC}^{\rm MEGA}$ continues to oscillate around $\delta_{\rm HC}^{\rm VMEC}$, confirming the agreement between the two codes. Here, we present only the detailed results for the $q_0/\rho_{\rm qmin}=1.1/0.57$ equilibrium. To ensure that the agreement between MEGA and VMEC in terms of $\delta_{\rm HC}$ holds in a broad range of equilibria, a similar comparison is performed for other equilibria among the q_0 and $\rho_{\rm qmin}$ scans. The quasi-steady state results for each equilibrium are summarized and shown in Fig.4(a-b). The results shown in this figure were calculated from the $0 \leq n \leq 1$ simulation to eliminate the contribution of the secondary mode. We find that MEGA always yields a higher $\delta_{\rm HC}$ than VMEC, but with a maximum difference of only 15%.

Benchmarking in terms of δ_{HC} is insufficient because it only represents the displacement of the magnetic axis. To benchmark in terms of overall structure, the bulk plasma pressure profile after HC formation is compared. We only show the results from the main reference equilibrium. Figure 4(c) compares the β_b profile along the geometric mid-plane at the $\phi=0^\circ$ toroidal angle. The VMEC result is plotted using a blue dashed line, while the gray and red solid lines represent the MEGA results at the axisymmetric state and quasi-steady state, respectively. We found that the β_b profile after the initial saturation phase predicted by MEGA (red solid line) agrees with that of VMEC (blue dashed line). In addition, we compare the β_b profile in the radial flux coordinate, as shown in Fig. 4(d), and find good agreement. Recalling that VMEC treats β_b as a prescribed input, this agreement confirms that the saturation of HC in MEGA remains in the proximity of ideal MHD physics.

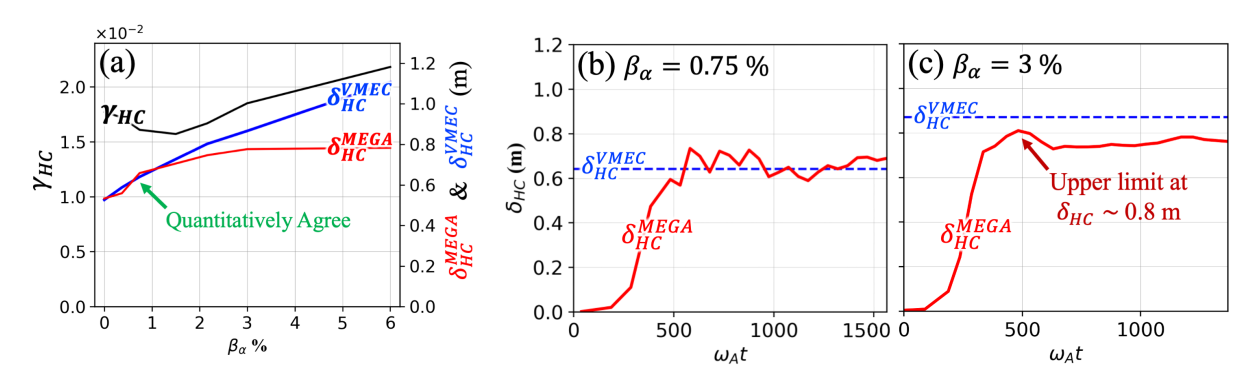


FIG. 5. Dependence of (a) the m/n=1/1 linear growth rate $\gamma_{\rm HC}$ and (b) the steady-state HC axis displacement $\delta_{\rm HC}$ on alpha pressure β_{α} . Panels (c) and (d) show the detailed time evolution of $\delta_{\rm HC}^{\rm MEGA}$ for the $\beta_{\alpha}=0.75\%$ and 3%. The red and blue colors represent the results calculated with MEGA and VMEC, respectively.

3.2. Effects of Alphas on HC Formation

In this section, fusion-born alpha is represented as a PIC in MEGA, while in VMEC, it is included only as an additional scalar MHD pressure. β_{α} is scanned over the $0\% < \beta_{\alpha} \leq 6\%$ range (ITER operates at $\beta_{\alpha} \sim 1\%$), following the profiles shown in Fig.2(a). To mitigate the complications caused by the secondary mode, we only consider the $n \leq 1$ simulation.

The dependence of the linear growth rate $\gamma_{\rm HC}$ of the m/n=1/1 mode on β_{α} is shown in Fig.5(a). Within $\beta_{\alpha}\leq 1\%$, alpha weakly reduces $\gamma_{\rm HC}$ by roughly 10%, likely due to the stabilization effect of trapped alphas[9]. If one increases β_{α} beyond 1%, $\gamma_{\rm HC}$ starts to increase, signifying the smooth transition to the EP branch.

The quasi-steady state results for $\delta_{\rm HC}$ are shown in Fig.5(b). The red and blue colors represent MEGA and VMEC results, respectively. Unlike $\gamma_{\rm HC}$ where there is a weak stabilization within the $\beta_{\alpha} \leq 1\%$ range, $\delta_{\rm HC}^{\rm MEGA}$ always increases. The decorrelation between $\gamma_{\rm HC}$ and $\delta_{\rm HC}$ is not surprising since the transition from the axisymmetric to the HC equilibrium involves strong quasi-linear and nonlinear effects that globally modify the equilibrium profiles.

To understand the role of alphas on HC formation, $\delta_{\rm HC}$ calculated by MEGA and VMEC is compared. As discussed in Section 2.2, VMEC cannot consider the kinetic effect of alpha; therefore, the contribution of alpha is included only as an additional scalar MHD pressure defined by Eq.8. The VMEC results are shown in Fig.5(a) as a blue solid line. Within the range of $0 \le \beta_{\alpha} \le 1\%$ (within ITER operating conditions), $\delta_{\rm HC}^{\rm MEGA}$ quantitatively agrees with that of VMEC. Within this range, $\beta_{\alpha} = 0.75\%$ is selected and its detailed time evolution of $\delta_{\rm HC}^{\rm MEGA}$ is shown in Fig.5(b). $\delta_{\rm HC}^{\rm MEGA}$ is shown as a red solid

line, while $\delta_{\rm HC}^{\rm VMEC}$ is shown as a blue dashed line. It can be seen that $\delta_{\rm HC}^{\rm MEGA}$ oscillates around $\delta_{\rm HC}^{\rm VMEC}$ after the saturation without any decay. This agreement may imply that the contribution of alphas to $\delta_{\rm HC}$ can be well approximated using an ideal MHD model.

If we increase β_{α} further beyond the ITER operating range, $\delta_{\rm HC}^{\rm MEGA}$ continues to grow until it reaches an upper limit of approximately $0.8~\rm m$ at $\beta_{\alpha} \geq 3.0\%$, as shown in Fig.5(a). In contrast, such a limit is not observed for $\delta_{\rm HC}^{\rm WEGA}$. The detailed time evolution of $\delta_{\rm HC}^{\rm MEGA}$ for the $\beta_{\alpha} = 3\%$ case is shown in Fig.5(c). It can be seen that $\delta_{\rm HC}^{\rm MEGA}$ has never exceeded this upper limit throughout the simulation. To understand this upper limit, we compare the quasi-steady state profile of $\beta_{\rm b}$, $\beta_{\alpha\parallel}$, and $\beta_{\alpha\perp}$ across all β_{α} scan cases. These profiles are compared along the geometric mid-plane at $\phi=0^{\circ}$, as shown in Fig.6. We begin with the analysis of the $\beta_{\rm b}$ profile shown in Fig.6(a). After HC formation, the $\beta_{\rm b}$ profile remains peaked for the $\beta_{\alpha}=0.37\%$ (violet) and 0.75% (cyan) cases. As one increases β_{α} further, a notable reduction in the β_{b} peak value can be observed, particularly in the $\beta_{\alpha}=3\%$ (yellow) and 6% (red) cases.

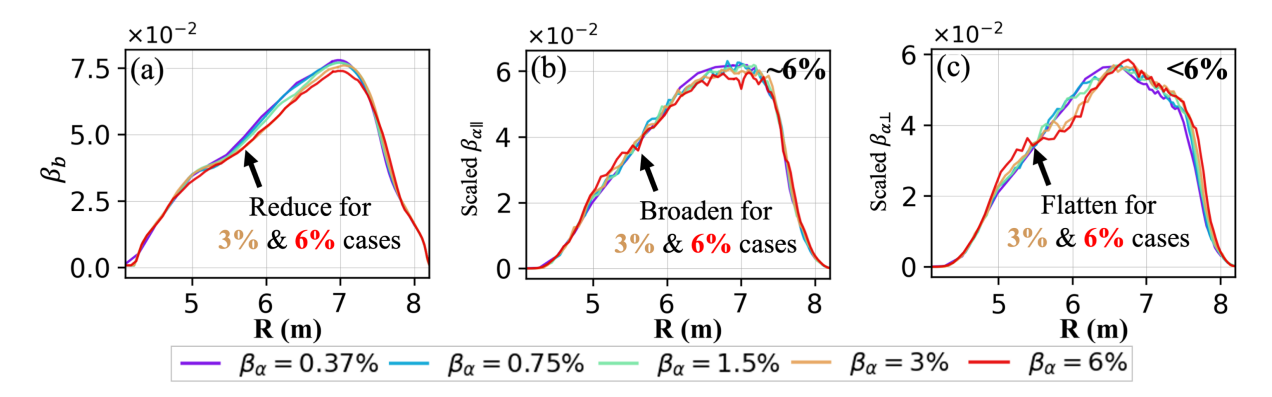


FIG. 6. Comparison of the (a) β_b , (b) scaled $\beta_{\alpha\parallel}$, and (c) scaled $\beta_{\alpha\perp}$ profiles along the geometric mid-plane at $\phi=0^\circ$ during the quasi-steady state for different β_α values. For clarity, the $\beta_{\alpha\parallel}$ and $\beta_{\alpha\perp}$ profiles of the $\beta_\alpha=0.37\%$, 0.75%, 1.5%, and 3% cases are scaled by a factor of 16, 8, 4, and 2, respectively.

For the $\beta_{\alpha\parallel}$ and $\beta_{\alpha\perp}$ profiles shown in Figs.6(b–c), the curves corresponding to $\beta_{\alpha}=0.37\%,\,0.75\%,\,1.5\%$, and 3% are amplified by factors of 16, 8, 4, and 2, respectively. This amplification makes the initial peak value for each case matches that of the $\beta_{\alpha}=6\%$ case, allowing a direct comparison. For the $\beta_{\alpha\parallel}$ profile, its peak value can be maintained for the $\beta_{\alpha}=0.37\%$ and 0.75% cases (On-axis scaled $\beta_{\alpha\parallel}\sim6\%$); however, a reduction is observed in the $\beta_{\alpha}\geq3\%$ cases (On-axis scaled $\beta_{\alpha\parallel}<6\%$).

For the $\beta_{\alpha\perp}$ profile, the reduction in peak value can be observed for all cases, as its on-axis scaled $\beta_{\alpha\perp}$ is less than 6%. In the $\beta_{\alpha} \geq 3\%$ cases, the $\beta_{\alpha\perp}$ profile exhibits a significant flattening. This flattening not only reduces the peak value further but also increases pressure anisotropy. These effects are not captured by the ideal MHD model, which explains the upper limit of $\delta_{\rm HC}^{\rm MEGA}$ and its deviation from VMEC. (Although the reduction in the $\beta_{\alpha\perp}$ peak is also observed in MEGA for all cases, its net effect remains small for the $\beta_{\alpha} \leq 1\%$ cases because β_{α} is relatively much smaller than β_b .)

4. PROPERTIES OF SECONDARY MODE

This section focuses on the stability of HC equilibrium, particularly the properties of the secondary mode ($5 \le n \le 8$). Fourier modes) observed in Section 3.1. We begin by investigating the spatial structure of the secondary mode in real space, as shown in Figs.7(a-b). This figure shows the poloidal cross-section of the perturbed MHD pressure profile δP_b at (a) $\phi = 0^\circ$, and (b) 180° toroidal angles. The overlaid black solid lines represent the magnetic Poincaré plot. The bold line represents the flux surface at q_{\min} . The secondary mode resides near q_{\min} , and it has a maximum fluctuation amplitude along the compressed flux region of HC. The toroidally and poloidally localized structure is preserved throughout its growth phase, suggesting that it is a single coherent mode. Recalling that the secondary mode emerges as the synchronized growth of the $5 \le n \le 8$ mode energies during $1400 \le \omega_A t \le 1800$ in Figs.3(a), these Fourier components must align such that they are interfere constructively in the compressed flux regions and destructively in the uncompressed flux regions.

Since the secondary mode comprises a broad spectrum of n>4 Fourier components, its structure may not be adequately represented with the $n\le 8$ simulation. Therefore, we calculate MEGA simulation directly from the HC equilibrium and turned off the toroidal low-pass filter. The results obtained with this method are shown in Figs.7(c-d). As a consequence, the δP_b fluctuation becomes more localized. If we performed a Fourier decomposition along the flux surface, this mode consists of a broad spectrum of m/n=(n+1)/n Fourier components. The dominant component is m/n=22/21, corresponding to q=1.047.

Lastly, we found that the secondary mode stability depends on the plasma resistivity. To quantify the stability of the secondary mode, its growth rate γ_{2nd} after its onset is measured. We scanned the normalized plasma resistivity $\hat{\eta} = \eta/(\mu_0 v_A R_0)$ within the $10^{-7} \le \hat{\eta} \le 10^{-4}$ range. At low $\hat{\eta}$, the numerical dissipation can be comparable to the physical dissipation;

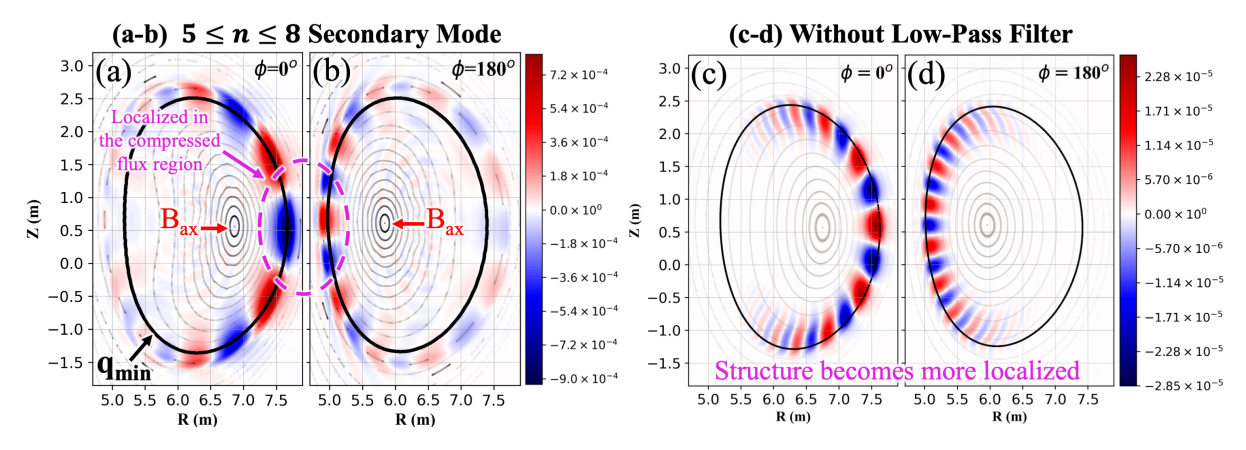


FIG. 7. Poloidal cross-section of the Perturbed MHD pressure profile δP_b at $(a,c) \phi = 0^{\circ}$ and $(b,d) 180^{\circ}$ toroidal angles. Panels (a-b) show the results from the $n \leq 8$ simulations, while panels (c-d) present the results initiated from the HC equilibrium without using a toroidal low-pass filter.

therefore, the simulation with enhanced grid resolution is required to ensure convergence. The scanned results are presented in Fig.8(a). The "×" and "+" markers denote simulations with the normal (N_R,N_Z) =(200,200) and enhanced poloidal resolutions (400,400), respectively. We find that the $5 \le n \le 8$ secondary mode becomes more unstable at higher $\hat{\eta}$, indicating its resistive nature. However, as mentioned previously, the $5 \le n \le 8$ Fourier components are insufficient to represent its actual structure. We perform a similar analysis in the simulation initiated from the HC equilibrium (turning off the low-pass filter), and the results are shown in Fig.8(b). Unlike the $5 \le n \le 8$ secondary mode, we observe a transition from a resistive secondary mode to an ideal secondary mode at low $\hat{\eta}$. This difference in secondary mode stability between the two cases may be attributed to the difference in the mode structure, specifically the short-wavelength spectrum, which strongly enhances instability.

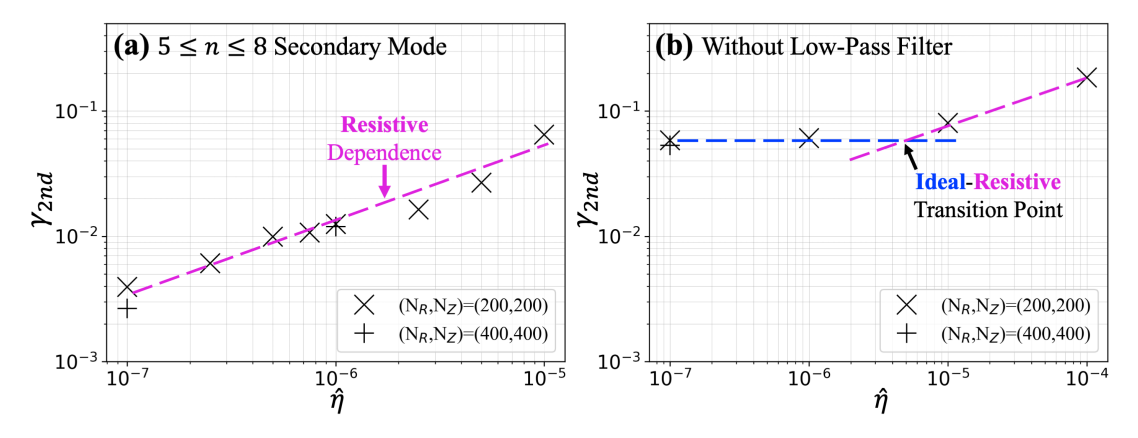


FIG. 8. Dependence of the secondary mode's growth rate γ_{2nd} on plasma resistivity $\hat{\eta}$. Panels (a-b) show the results from the $n \leq 8$ simulations, while panels (c-d) present the results initiated from the HC equilibrium without using a toroidal low-pass filter.

The results in this section reveal the qualitative nature of the secondary mode; however, there is a high possibility that some of these findings may differ from actual experiments. One of our primary concerns stems from its short-wavelength structure (e.g., m/n=22/21 and beyond), which is smaller than the validity of the MHD scale length. Additionally, the χ_{\parallel} used in our study is insufficient for simulating rapid plasma relaxation along the magnetic field line. This small χ_{\parallel} then may exaggerate the short-wavelength mode.

5. CONCLUSION

The transition from the axisymmetric equilibrium to the HC equilibrium in ITER-scale plasmas with fusion-born alphas was studied using MEGA (a nonlinear MHD-PIC code) and VMEC (3-D ideal MHD equilibrium solver). Since these two codes incorporate different physical models, comparing the HC solution calculated with MEGA and VMEC can provide insight into the mechanism of HC formation and the roles of alphas. We find that the core toroidal asymmetry, represented by the n=1 displacement of the magnetic axis, $\delta_{\rm HC}$, tends to increase with alpha pressure β_{α} . Within the ITER operating range of

IAEA-CN-392/INDICO ID TH-W07 (PREPRINT)

alpha pressure, $\beta_{\alpha} \leq 1\%$, the non-ideal effects are sufficiently small; therefore, the contribution of alphas can be approximated using a fluid model. At higher $\beta_{\alpha} > 1\%$, the non-ideal effects become increasingly important, resulting in a notable cross-field transport. The contribution of alphas then required a kinetic description.

Lastly, we presented preliminary results on the MHD instability in HC equilibrium. MEGA predicts an unstable short-wavelength mode localized along the compressed flux region of HC, capable of causing widespread magnetic chaos. However, the physics of this mode is likely to fall outside the valid range of MHD theory; therefore, it should be re-evaluated using a more appropriate model.

REFERENCES

REFERENCES

- [1] WA Cooper et al. "Tokamak Magnetohydrodynamic Equilibrium States with Axisymmetric Boundary and a 3D Helical Core". In: *Physical Review Letters* 105.3 (2010), p. 035003.
- [2] P Piovesan et al. "Role of a continuous MHD dynamo in the formation of 3D equilibria in fusion plasmas". In: *Nuclear Fusion* 57.7 (2017), p. 076014.
- [3] D Pfefferlé et al. "NBI fast ion confinement in the helical core of MAST hybrid-like plasmas". In: *Nuclear Fusion* 54.6 (2014), p. 064020.
- [4] IT Chapman et al. "Saturated ideal modes in advanced tokamak regimes in MAST". In: *Nuclear Fusion* 50.4 (2010), p. 045007.
- [5] A Wingen et al. "Use of reconstructed 3D equilibria to determine onset conditions of helical cores in tokamaks for extrapolation to ITER". In: *Nuclear Fusion* 58.3 (2018), p. 036004.
- [6] Y Nakamura, A Ishizawa, and Y Ishida. "Influence of plasma boundary shape on helical core/long-lived mode in tokamak plasmas". In: *Physics of Plasmas* 27 (2020), p. 092509.
- [7] SP Hirshman and JC Whitson. "Steepest-descent moment method for three-dimensional magnetohydrodynamic equilibria". In: *The Physics of Fluids* 26.12 (1983), pp. 3553–3568.
- [8] K McGuire et al. "Study of high-beta magnetohydrodynamic modes and fast-ion losses in PDX". In: *Physical Review Letters* 50.12 (1983), p. 891.
- [9] F Porcelli. "Fast particle stabilisation". In: Plasma Physics and Controlled Fusion 33.13 (1991), p. 1601.
- [10] Y Todo and T Sato. "Linear and nonlinear particle-magnetohydrodynamic simulations of the toroidal Alfvén eigenmode". In: *Physics of Plasmas* 5.5 (1998), pp. 1321–1327.
- [11] SH Kim et al. "CORSICA modelling of ITER hybrid operation scenariosb". In: *Nuclear Fusion* 56.12 (2016), p. 126002.